Korean J. Chem. Eng., 35(11), 2207-2219 (2018)
DOI: 10.1007/s11814-018-0145-2

pISSN: 0256-1115
eISSN: 1975-7220

Removal characteristics of chromium by activated carbon/$CoFe_2O_4$ magnetic composite and *Phoenix dactylifera* stone carbon

Rauf Foroutan*, Reza Mohammadi*, Bahman Ramavandi,†, and Maryam Bastanian***

*Polymer Research Laboratory, Department of Organic and Biochemistry, Faculty of Chemistry, University of Tabriz, 5166616471 Tabriz, Iran
**Department of Environmental Health Engineering, Faculty of Health and Nutrition, Bushehr University of Medical Sciences, Mobaraki Street, 7518759577 Bushehr, Iran
(*Received 26 June 2018 • accepted 23 August 2018*)

Abstract−Activated carbon (AC) was synthesized from *Phoenix dactylifera* stones and then modified by $CoFe_2O_4$ magnetic nanocomposite for use as a Cr(VI) adsorbent. Both AC/$CoFe_2O_4$ composite and AC were fully characterized by FTIR, SEM, XRD, TEM, TGA, and VSM techniques. Based on the surface analyses, the addition of $CoFe_2O_4$ nanoparticles had a significant effect on the thermal stability and crystalline structure of AC. Factors affecting chromium removal efficiency like pH, dosage, contact time, temperature, and initial Cr(VI) concentration were investigated. The best pH was found 2 and 3 for Cr adsorption by AC and AC/$CoFe_2O_4$ composite, respectively. The presence of ion sulfate had a greater effect on the chromium sorption efficiency than nitrate and chlorine ions. The results illustrated that both adsorbents can be used up to seven times to adsorb chromium. The adsorption process was examined by three isothermal models, and Freundlich was chosen as the best one. The experimental data were well fitted by pseudo-second-order kinetic model. The half-life ($t_{1/2}$) of hexavalent chromium using AC and AC/$CoFe_2O_4$ magnetic composite was obtained as 5.18 min and 1.52 min, respectively. Cr(VI) adsorption by AC and AC/$CoFe_2O_4$ magnetic composite was spontaneous and exothermic. In general, our study showed that the composition of $CoFe_2O_4$ magnetic nanoparticles with AC can increase the adsorption capacity of AC from 36 mg/L to 70 mg/L.

Keywords: Activated Carbon, AC/$CoFe_2O_4$ Composite, Chromium Adsorption, Desorption Study, Half-life

INTRODUCTION

The pollution of water bodies by toxic heavy metals is one of the most serious environmental issues in the world. Disposal of untreated wastewaters containing heavy metals has a detrimental impact on the ecosystem and human health [1]. Chromium as one of the toxic heavy metals has extensively been used in industries, including electroplating, leather tanning, metal plating, battery, and petroleum refining [2,3]. In aqueous environments, the chromium metal exists in two oxidation states of trivalent (Cr(III)) and hexavalent (Cr(VI)). The Cr(VI) form is more toxic than Cr(III) and is a suspected carcinogenic material. Hexavalent chromium is very soluble and mobile in the natural environment [4]. The World Health Organization (WHO) has recommended the maximum allowable value of 0.1 mg/L and 0.05 mg/L for Cr(VI) in drinking water and potable water, respectively [5]. So, the treatment of the Cr(VI) contaminated effluents before discharge to the water bodies and ecosystems is very important.

There are several strategies for Cr(VI) treatment, including membrane separation, reduction, chemical precipitation, ion exchange, and adsorption [6]. Adsorption is preferred for Cr(VI) removal due to its flexibility in operations, high efficiency, the capability of recycling both adsorbent and adsorbate (if desired), the simplicity of design, and it does not generate secondary pollutant during operations [7]. Different adsorbents such as bone char-ZnO [8], zeolites [9], clay [10], polymer [11], and activated carbon [12] have been tested for removal of Cr(VI) from aqueous solution. Among them, activated carbon has gained more attention due to the high surface area, fast kinetics, high efficiency, and facile regeneration. As commercial activated carbon is expensive, preparation of activated carbon from low or no cost materials can reduce the overall cost of the treatment by activated carbon. Several researchers have used activated carbon derived from apple peels [13], date press cake [14], chestnut oak shells [15], and tea waste biomass [16] for chromium removal.

In recent years, spinel ferrite nanoparticles have received considerable attention due to their ease of separation under external magnetic fields [17]. Among the spinel ferrite compounds, much efforts have been undertaken on the synthesis of cobalt ferrite ($CoFe_2O_4$), because of its chemical stability, large surface to volume ratio, high mechanical hardness, high magneto crystalline anisotropy ($k>10^5$ J/m^3), and coercivity [18,19]. Magnetization capability in $CoFe_2O_4$ can be used in activated carbon to make the adsorption process more efficient. Although $CoFe_2O_4$ in composition with activated carbon as an adsorbent material has rarely been used for water purification [20,21], there is no comprehensive information on the properties of the activated carbon/$CoFe_2O_4$ composite and kinetics (including contaminant half-life). Further, to reduce costs and present an environmental friendly adsorbent, the composition of

†To whom correspondence should be addressed.
E-mail: ramavandi_b@yahoo.com, b.ramavandi@bpums.ac.ir

$CoFe_2O_4$ and activated carbon prepared from natural materials has not yet been tested to remove contaminants. One of the natural biomasses that are abundantly used to produce activated carbon is *Phoenix dactylifera* date stones [22,23]. The date stones of *P. dactylifera* have a good feature, such as availability, cost-free, easy bonding with metals, and low toxicity. The activated carbon (AC) provided from *P. dactylifera* date stones has not been modified with cobalt ferrite to remove pollutants. Therefore, the results of the application of AC-cobalt ferrite may be interesting to the scientific community.

Thus, the purposes of the current work were design to produce the activated carbon (AC) from *P. dactylifera* date stones and then composite with $CoFe_2O_4$, examine the potential of AC and AC/$CoFe_2O_4$ composite as an adsorbent for the Cr(VI) removal, fully characterize the properties of AC and AC/$CoFe_2O_4$ using energy dispersive X-ray spectroscopy (EDX), mapping, scanning electron microscopy (SEM), Fourier transform infrared spectrometry (FT-IR), X-ray diffraction (XRD), transmission electron microscopy (TEM), thermogravimetric analyzer (TGA), and vibrating sample magnetometer (VSM) techniques, and study the kinetics, isotherms, half-life and affecting physicochemical factors on the Cr removal by AC and AC/$CoFe_2O_4$ composite.

EXPERIMENTAL

1. Preparation of Synthetic Solution

All the materials used were laboratory grade and used without purification. The stock solution of Cr(VI) with a concentration of 1,000 mg/L was obtained by dissolving 2.8289 g of potassium dichromate ($K_2Cr_2O_7$) in the deionized water. The solution was diluted with deionized water to prepare a solution with a specific initial concentration of chromium ion. To adjust the pH of solutions, diluted 0.1 M HCl or NaOH was used. All chemicals used in this work were purchased from Merck Company (Germany) and the deionized water was used to prepare solutions for all tests.

2. Preparation of Adsorbents

In this study, the dates of *Phoenix dactylifera* were used for the production of activated carbon. Dates were provided from local confectionary without any cost. In the laboratory, the stones were washed with water to remove excess materials. After washing, data stones (30 g) were placed in an oven at 400 °C for 2 h for carbonization. After that, the carbonized date stones were ground using a powder mill and placed in sodium hydroxide solution to be activated. After the activated carbon was separated from the solution, it was placed in an oven at 700 °C for 2 h. The heating rate was fixed at 5 °C/min. Then, the achieved activated carbon was removed from the oven and placed at ambient temperature to be cooled and finally washed with distilled water several times to completely neutralize (pH 6.5-7.5).

A chemical deposition method was used to produce the magnetic composite of AC/$CoFe_2O_4$. First, a liquid solution (200 mL) containing cobalt (II) (2.379 g of $CoCl_2{\cdot}6H_2O$) and iron (III) (3.244 g of $FeCl_3$) with a molar ratio of 1 : 2 was prepared. Then, 2.5 g of AC produced from the *P. dactylifera* stones was added and stirred for 20 min to bring iron and cobalt ions to the AC pores. After that, the solvent temperature was increased to 80-90 °C. Under these conditions, NaOH solution (3 M, 50 mL) was added dropwise to the mixture and stirred for 120 min under nitrogen gas. The formed magnetic composite of AC/$CoFe_2O_4$ was removed from the solution using a magnetic field (magnet) and washed several times with deionized water to completely neutralize (pH 6.5-7.5). After neutralization, the composite was placed in an oven for 24 h at 105 °C to completely dried and then used as an adsorbent for removing Cr(VI) ions.

3. Characterization of the Adsorbents

To investigate the surface changes of AC and AC/$CoFe_2O_4$ composite before and after Cr(VI) adsorption, the SEM, EDX, and mapping analysis was seen by using the scanning electron microscope (SEM-TESCAN MIRA3-FEG). The functional groups on the surface of adsorbents and the interaction between the existing functional groups and Cr(VI) after the adsorption process were determined using the FT-IR spectrometer (Broker victor 22) over the wave number range of 400-4,000 cm^{-1}. The XRD patterns of AC and AC/$CoFe_2O_4$ composite were performed using a Siemens D 500 diffractometer with Cuk_α radiation (35 kV, λ=1.5048 A°) in the 2θ range of 5-80° at a scanning rate of 1°/min. Transmission electron microscopy (TEM) was done using an LEO 906 microscope at 80 kv. The thermogravimetric analyzer (TGA) was used to study the thermal stability of adsorbents. In this method, the change in the weight of adsorbents was determined as a function of temperature and under specific temperature control conditions. This analysis was carried out using a TGA-PL analyzer (TGA 1500 model, England). To determine the magnetic properties of $CoFe_2O_4$ nanoparticles and AC/$CoFe_2O_4$ composite, a vibrating sample magnetometer (VSM) analysis was performed with a magnetic field in the range of –8,000 to 8,000 Oe by using a VSM (MPMS-5 SQUID). The pH of zero charge point (pHzpc) for AC and AC/$CoFe_2O_4$ composite was obtained by stirring 0.25 g of the adsorbents with 100 mL of CO_2-free double distilled water, according to the pH drift procedure.

4. Adsorption Experiments

Cr(VI) ions experiments were carried out using AC and AC/$CoFe_2O_4$ composite in a batch mode in 250 mL Erlenmeyer flasks containing 100 mL of solution. The effect of parameters such as initial pH, dose of adsorbent, initial Cr concentration, solution temperature, and contact time was investigated. For this purpose, the batch adsorption experiments were performed in the laboratory conditions of 1 g/L dose of adsorbent, 10 mg/L initial chromium concentration, 60 min contact time, 25 °C temperature, and 400 rpm stirring speed. After the optimum pH was determined, the influence of other parameters was studied at this pH and initial concentration of 10-100 mg/L Cr(VI), 0.5-5 g/L adsorbent dose, and 5-130 min contact time. The effect of co-existing anion was also performed at Cr(VI) concentration of 10 mg/L, adsorbent dose of 1.5 g/L, pH of 2 (for AC) and 3 (for AC/$CoFe_2O_4$) and the ionic medium ($NaNO_3$, $NaSO_4$, and NaCl) concentration of 10 mg/L. After the given contact time, the solution was filtered using Whatman 42 papers, and 20 mL of filtrate was stored to analyze the residual Cr(VI) by an atomic absorption spectroscopy (novAA400, Analytick Jena, Germany) equipped with acetylene-air fuel. The removal percentage (R, %) and adsorption capacity (q_e, mg/g) were calculated according to the following equations:

$$R(\%)=\left(\frac{C_{in}-C_{fi}}{C_{in}}\right)\times 100 \quad (1)$$

$$q_e=\left(\frac{C_{in}-C_{fi}}{W}\right)\times V \quad (2)$$

where: C_{in} and C_{fi} (mg/L) are the initial and final concentration of chromium, respectively, V (L) is the volume of solution, and W (g) is the mass of AC or AC/$CoFe_2O_4$.

5. Desorption and Reuse Study

For desorption study, the amount of 1.5 g/L adsorbent (active carbon or AC/$CoFe_2O_4$ magnetic composite) to a solution containing 10 mg/L chromium (VI) in conditions such as optimal pH, mixing speed of 400 rpm, temperature 25 °C, and the contact time of 60 min. After the completion of the reaction time, the adsorbents were separated from the aqueous solution and washed twice with distilled water to remove excess ions of chromium metal (VI) at the adsorbent surface. The adsorbent was dried at 105 °C. Then, the dried adsorbents were poured into 100 mL of NaOH solution with various concentrations (0.05-0.5 M) and stirred for 120 min. At the end of this time, the adsorbent was separated from the aque-

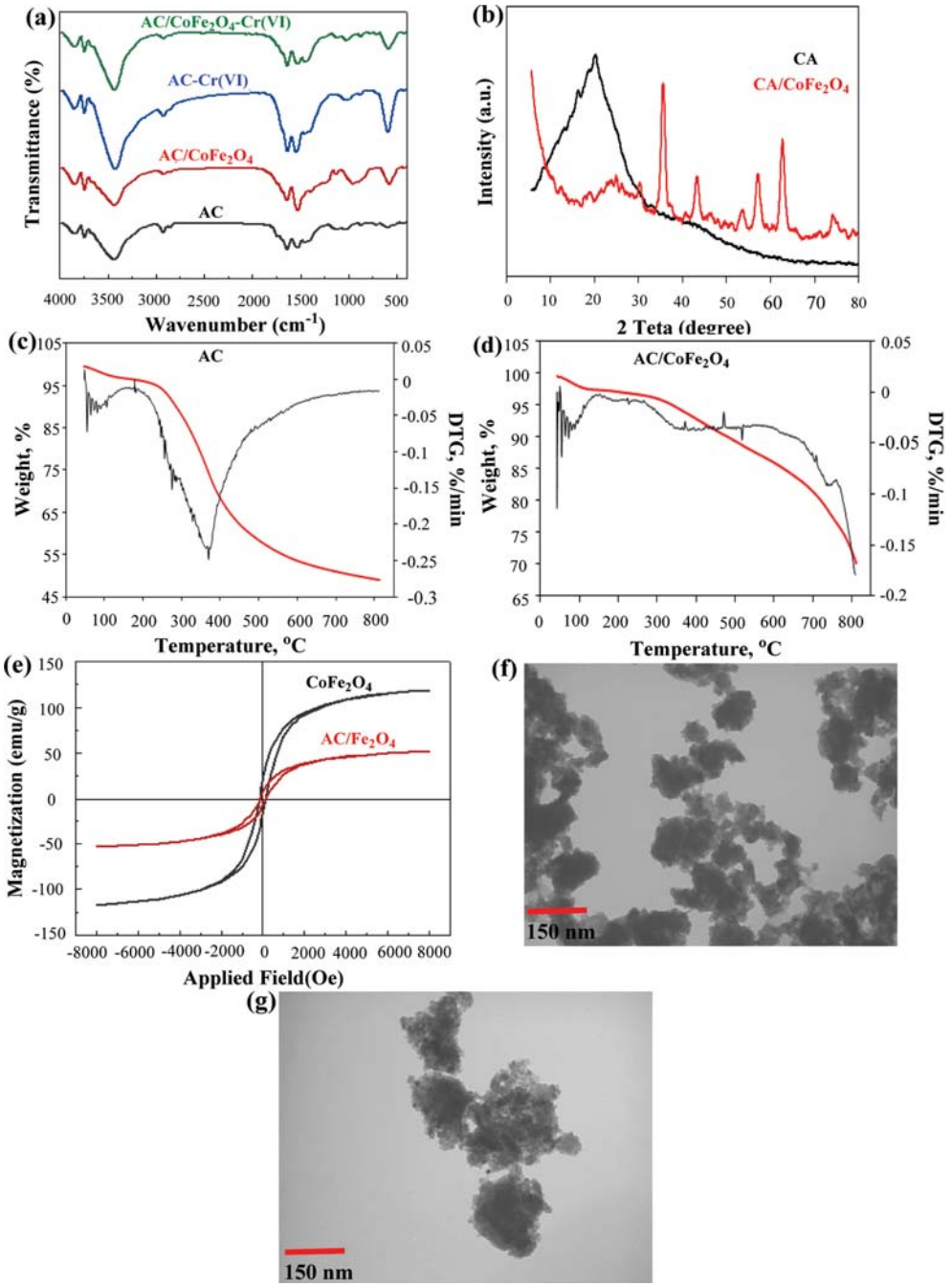

Fig. 1. FT-IR spectrum before and after Cr(VI) adsorption (a), XRD pattern (b), TGA-DTG plots (c), (d), hysteresis loop for AC and AC/$CoFe_2O_4$ composite (e), TEM image of AC (f), and TEM image of AC/$CoFe_2O_4$ composite (g).

ous solution and the concentration of chromium ion (VI) was measured. Desorption test was carried out to seven stages and the adsorption efficiency of the adsorbents was studied. The percentage of desorption was determined using the following equation:

$$\text{Desorption (\%)} = 100 \times \left(\frac{\text{The amount of Cr(VI) desorbed}}{\text{The amount of Cr(VI) adsorbed}} \right) \quad (3)$$

RESULTS AND DISCUSSION

1. Characterization

To understand the main functional groups of the reacted and non-reacted AC and AC/$CoFe_2O_4$ composite, the FT-IR method was used (Fig. 1(a)). The broad and strong peak at the range of 3,437-3,742 cm^{-1} may be attributed to the hydroxyl (OH) or amine (-NH_2) groups of adsorbents. The characteristic peaks at the range of 1,637-1,739 cm^{-1} and 1,033-1,527 cm^{-1} may be due to the symmetric and antisymmetric carboxyl group and the (-C-O) group, respectively [24]. Also, there are peaks at 872 and 956 cm^{-1} which show the presence of -CN and S=O groups in the AC provided from *P. dactylifera* date stones and AC/$CoFe_2O_4$ structure. In AC/$CoFe_2O_4$, the presence of a courier at 574 cm^{-1} is probably due to the Fe-O vibrations [25]. This courier can confirm the formation of $CoFe_2O_4$ magnetic particles in the active carbon structure produced from the *P. dactylifera* date stones.

As shown in Fig. 1(a), significant changes happened during the vibration of the functional groups after Cr(VI) adsorption. The peaks related to OH or NH_2 and carboxyl groups were shifted to the range of 3,435-3,741 cm^{-1} and 1,524-1,642 cm^{-1}, respectively. Also, the new peaks at 874 and 1,022 cm^{-1} might be due to the Cr-O and Cr=O bands in the AC/$CoFe_2O_4$ composite. These peaks can be also seen in AC (976 and 1,130 cm^{-1}) [26].

The XRD patterns of activated carbon and AC/$CoFe_2O_4$ composite are depicted in Fig. 1(b). For AC adsorbent two broad peaks were found at around 2θ=20.21° and 2θ=43.61°. The lack of a sharp peak in AC adsorbent represents its amorphous structure. However, these peaks show that as much as possible impurities have been lost and have found the same crystalline structure as graphite. In the structure of AC/$CoFe_2O_4$ composite, there are peaks in the scattering range (2θ) at 18.66° (111), 29.96° (220), 35.26° (311), 42.86° (222), 46.51° (400), 53.21° (422), 56.81° (511), and 62.51° (440), which are indicative of the cubic inverse spinel type $CoFe_2O_4$ [18]. The intensity and place of the AC peaks are lowered after the composition with $CoFe_2O_4$, revealing the involvement of carbon with $CoFe_2O_4$ nanoparticles and the destruction of its crystalline structure [18].

TGA and DTG analyses were used to study the thermal stability of activated carbon and AC/$CoFe_2O_4$ nanocomposite, and the results are presented in Fig. 1(c), (d). Three mass decrease steps are visible in this figure. The first step is because of adsorbed water loss in the range of 50-100 °C [27]. The weight loss in AC at 267 °C refers to decomposing of AC, while AC/$CoFe_2O_4$ composite started decomposing in the range of 300-400 °C. The weight loss in this stage may be due to the decomposition of the adsorbents into condensable gas (acetic acid or methanol) and incondensable gases like carbon dioxide, methane, water, hydrogen. Similar reports have been found in the literature [28,29]. The third stage can be attributed to the deformation of AC and AC/$CoFe_2O_4$ composite. Also, it can be observed that the overall weight loss of AC (50.53%) was higher than AC/$CoFe_2O_4$ composite (29.35%). Therefore, the addition of $CoFe_2O_4$ nanoparticles has a significant effect on the thermal stability of activated carbon.

The magnetic properties of $CoFe_2O_4$ nanoparticles and AC/$CoFe_2O_4$ composite were assessed using a vibrating sample magnetometry, and the results of their hysteresis loops are represented in Fig. 1(e). The findings show that $CoFe_2O_4$ nanoparticles have higher saturation magnetization (Ms) values compared to AC/$CoFe_2O_4$ magnetic composite, and both materials have a ferromagnetic behavior. The maximum magnetic saturation value for $CoFe_2O_4$ nanoparticles and AC/$CoFe_2O_4$ magnetic magnets was found as 119.16 emu/g and 53.06 emu/g, respectively. The decrease in magnetic saturation can be attributed to factors such as particle size, and presence and concentration of oxygen adsorbed on AC/$CoFe_2O_4$ composite particles [30]. Note that the amount of remanence (Mr) and coercivity (Mc) parameters for $CoFe_2O_4$ nanoparticles was obtained as 18.68 emu/g and 154.36 emu/g, respectively, and for AC/$CoFe_2O_4$ composite were determined as 7.38 emu/g and 141.92 emu/g, respectively.

TEM images of AC and AC/$CoFe_2O_4$ composite are shown in Fig. 1(f), (g). It can be seen that activated carbon is agglomerated, and after being composited by $CoFe_2O_4$ it forms nanosized particles with a size of <150 nm. Also, TEM image (Fig. 1(g)) shows that most of the $CoFe_2O_4$ nanoparticles are uniformly distributed in the activated carbon matrix. All TEM findings were supported the XRD and SEM results.

2. SEM-EDX Study

The morphology of activated carbon and AC/$CoFe_2O_4$ composite before and after Cr(VI) adsorption was studied by SEM observation. Fig. 2(a) shows that AC has a smooth surface with a number of non-uniform cracks and holes. After Cr(VI) adsorption (Fig. 2(d)), the AC surface has become coarse and chromium ions have occupied inside the pores. Fig. 2(g) indicates that the surface of AC/$CoFe_2O_4$ composite is agglomerated and has many spherical particles and holes. By comparison Fig. 2(d) and Fig. 2(j), it is clear that more Cr(VI) have trapped in the AC/$CoFe_2O_4$ pores and hence, a more packed structure has resulted [18]. EDX and mapping findings also confirm these interpretations.

3. Parameters Evaluation

3-1. pH of Working Solution

The solution pH is an important operational parameter in the Cr adsorption process because it can be effective on the solubility of metal ions, the formation of opposite ions in functional groups, and also the degree of adsorbent ionization [31]. A batch adsorption test of Cr(VI) ions using AC and AC/$CoFe_2O_4$ composite was done in the initial pH range of 2-9, and the adsorption percentage of chromium (VI) metal ions was determined (Fig. 3(a)). Maximum adsorption efficiency of Cr(VI) ions was determined using AC (89.65%) and AC/$CoFe_2O_4$ composite (95.71%) at initial pH of 2 and 3, respectively. According to the results, the adsorption of Cr(VI) is pH-dependent and with increasing the initial pH, the adsorption efficiency of Cr(VI) ions was decreased for both adsorbents. At initial pH of 9, the adsorption efficiency was minimized.

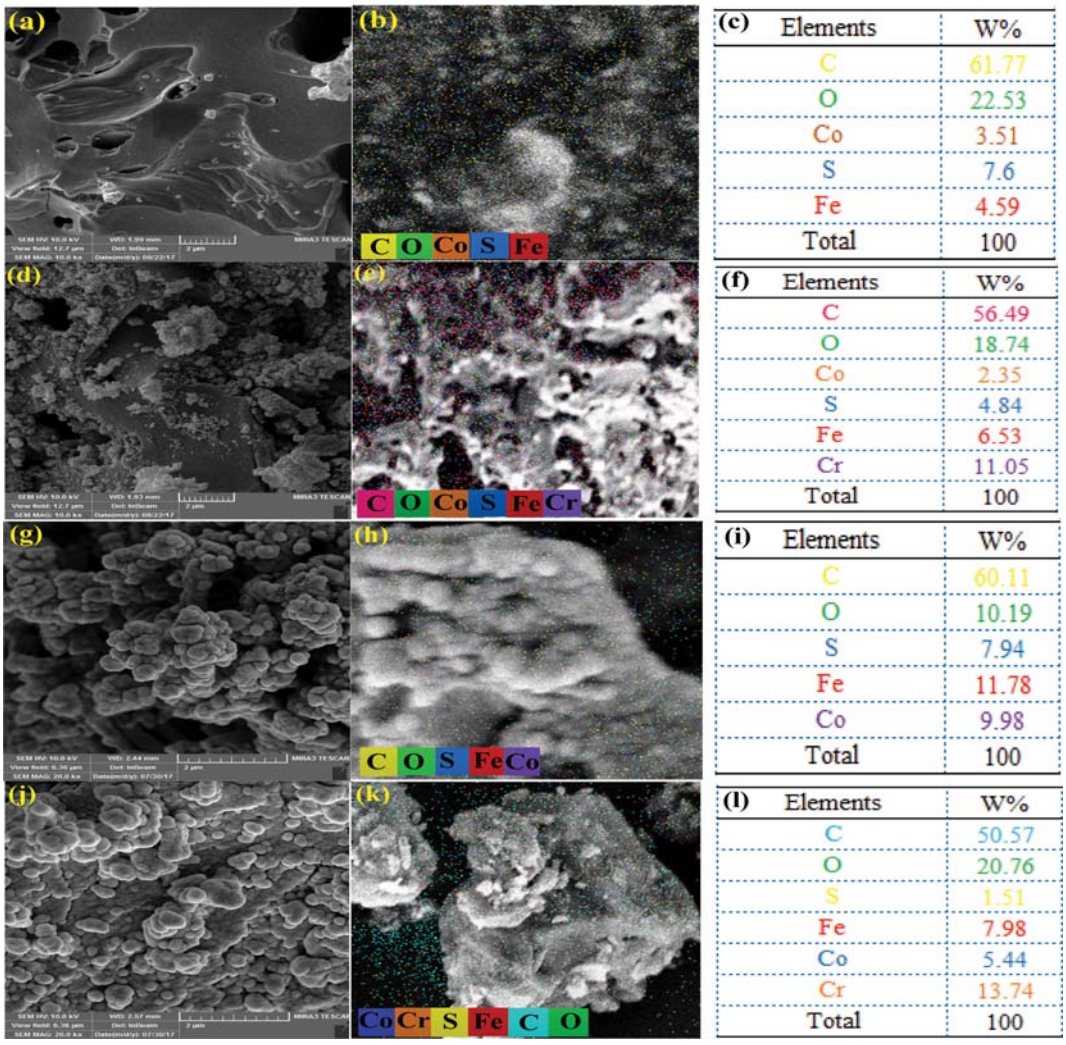

(c) Elements	W%
C	61.77
O	22.53
Co	3.51
S	7.6
Fe	4.59
Total	100

(f) Elements	W%
C	56.49
O	18.74
Co	2.35
S	4.84
Fe	6.53
Cr	11.05
Total	100

(i) Elements	W%
C	60.11
O	10.19
S	7.94
Fe	11.78
Co	9.98
Total	100

(l) Elements	W%
C	50.57
O	20.76
S	1.51
Fe	7.98
Co	5.44
Cr	13.74
Total	100

Fig. 2. SEM, mapping, and EDX of fresh AC (a)-(c), used AC (d)-(f), fresh AC/$CoFe_2O_4$ (g)-(i) and used AC/$CoFe_2O_4$ (j)-(*l*).

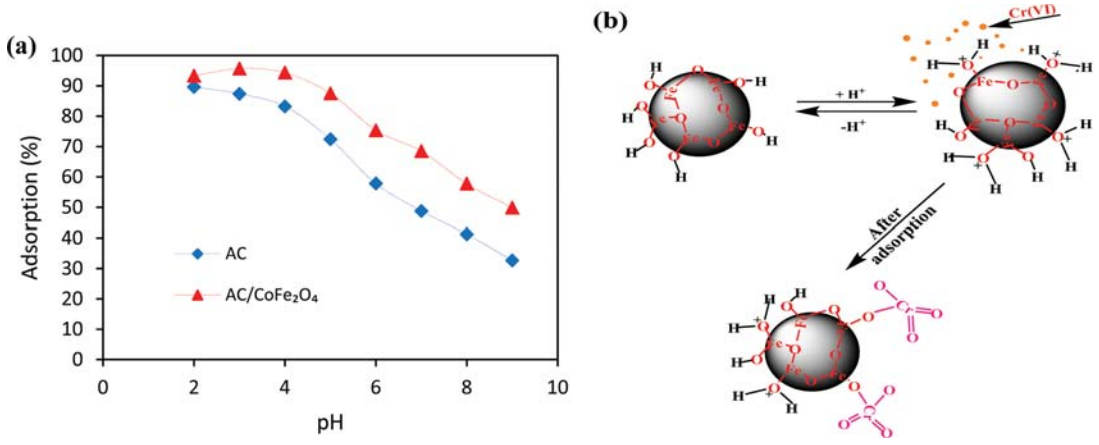

Fig. 3. (a) The effect of pH on Cr(VI) removal and (b) scheme of $HCrO_4^-$ ion adsorption onto adsorbents.

Chromium (VI) at different pH can be present in anionic forms such as $HCrO_4^-$, $Cr_2O_7^{2-}$, and CrO_4^{2-}. The dominant chromium ion in the initial pH range of 2 to 6 is $HCrO_4^-$ and $Cr_2O_7^{2-}$ that by increasing the initial pH of more than 6, the anionic form gradually turns into CrO_4^{2-} [32]. CrO_4^{2-} ion requires two active sites to be placed on the adsorbent surface due to the double negative charge, while $HCrO_4^-$ ions need only one active site. Also, the size of the $HCrO_4^-$ ion (44 cm^3/mol) compared to the size of the $Cr_2O_7^{2-}$ ion

(73 cm^3/mol) is smaller [33]. Thus, this form of chromium ion can easily penetrate into adsorbent layers and active sites and be placed on them. Another reason to increase the adsorption efficiency of chromium (VI) ion in acidic environments can be due to the adsorbent surface charge on alkaline environments. In acidic environments, the surface of the adsorbent has a positive charge (H^+) and the electrostatic force is produced by the gravity between the adsorbent and $HCrO_4^-$ ion, which can increase the adsorption efficiency (see Fig. 3(b)). In alkaline environments, the concentration of negative charge (OH^-) in the environment and the adsorbent surface increases. Thus, due to the co-occurrence of adsorbent surface charges and CrO_4^{2-} ion, an electrostatic repulsion force is produced, which results in lower efficiency. Also, OH^- ion will compete with metal ion for adsorption on the surface. This description is also in agreement with the amount of the pHzpc (AC=6.2 and AC/$CoFe_2O_4$=6.3). At working pHs<pHzpc, the adsorbent surface charge is positive and thus more Cr(VI) ions are adsorbed. Therefore, optimal pH for chromium removal using AC and AC/$CoFe_2O_4$ composite was determined to be 2 and 3, respectively.

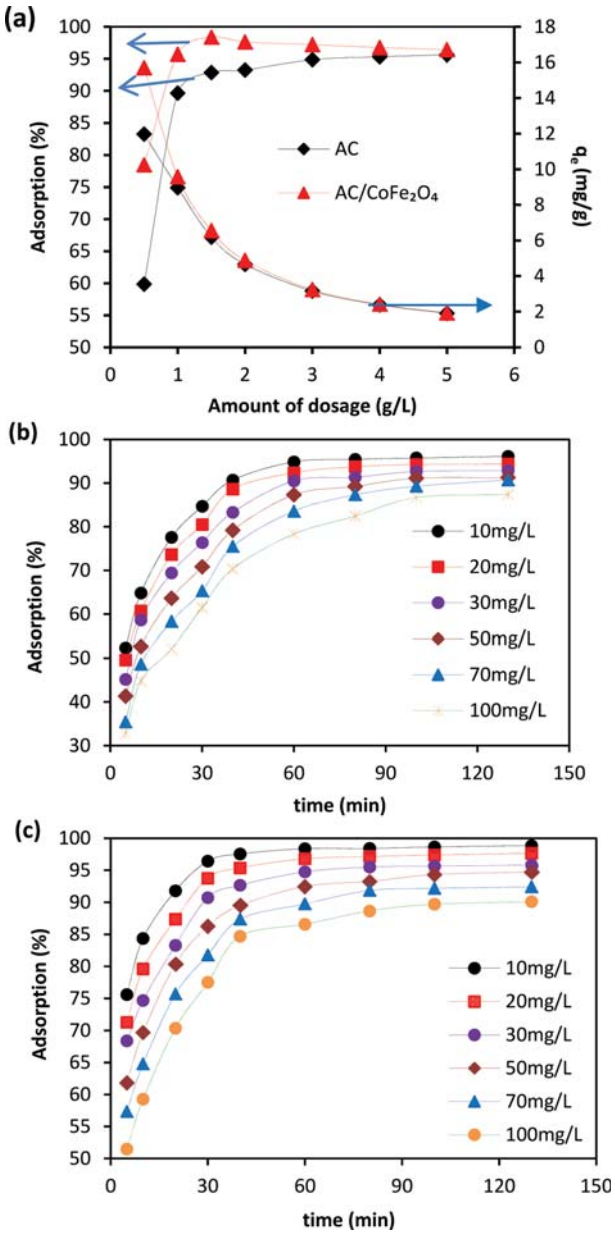

Fig. 4. The effect of adsorbent dose (a) and contaminant concentration-contact time during Cr adsorption by AC (b) and AC/$CoFe_2O_4$ composite (c).

3-2. Adsorbent Dosage

The effect of AC and AC/$CoFe_2O_4$ composite dose was studied at the conditions of adsorbent dose 0.5-5 g/L, temperature 25 °C, contact time 60 min, initial chromium concentration 10 mg/L, and optimal pH. The results are shown in Fig. 4(a). According to the results, in the initial dosage of the adsorbents (<2 g/L), the removal efficiency is rapidly increased and then remains almost constant. The maximum Cr removal for AC (94.87%) and AC/$CoFe_2O_4$ (98.38%) was seen at a dose of 3 g/L and 1.5 g/L, respectively. This increase in efficiency with increasing the dose could be justified by the availability of a sufficient surface and active sites [34]. The adsorption efficiency was not significantly altered after 3 g/L AC and 1.5 g/L AC/$CoFe_2O_4$ composite due to the aggregation of adsorbent particles, thereby reducing the effective surface area to adsorb metal ions [35].

Fig. 4(a) clearly demonstrates that the adsorption capacity is rapidly reduced with increasing dose of adsorbents. Two plausible reasons for this issue are:

- High amounts of adsorbents make accessible active sites to adsorb contaminants. Since the concentration of metal ion in aqueous solution is constant, not all active adsorbent sites will be used by increasing the adsorbent dosage; and
- Increasing the adsorbent dose causes the adsorbent particles to collide with each other and creates an aggregated mass, which reduces the total surface area, the number of active sites, and increases the length of adsorbate penetration path [36,37].

3-3. Contact Time and Initial Cr(VI) Concentration

The impact of contaminant concentration-contact time on the adsorption percentage of chromium (VI) using activated carbon and AC/$CoFe_2O_4$ magnetic composite was investigated (Fig. 4(b), (c)). The tests were performed at contact time 5-130 min, initial chromium concentration 10-100 mg/L, solution temperature 25 °C, adsorbent dose 3 g/L (for AC) and 1.5 g/L (for AC/$CoFe_2O_4$), and optimal initial pH. According to the results, the majority of the chromium ions were adsorbed at the initial contact times; while after 60 min for AC and 40 min for AC/$CoFe_2O_4$, the Cr(VI) adsorption occurred in a slower mode. The high adsorption rate at the initial contact time resulted from the vacancy of a large number of active sites in the adsorbent surface. Therefore, the optimum contact time for the chromium sorption process using activated carbon and activated carbon/$CoFe_2O_4$ was determined as 60 min and 40 min, respectively.

The effect of initial concentration of Cr(VI) ions on the efficiency of the Cr adsorption process is also depicted in Fig. 4(b), (c). Results show that by increasing the initial concentration of chromium ions, the adsorption efficiency for both adsorbents decreases. Reducing the adsorption efficiency by increasing the Cr concentration can be due to the saturation of active sites in the adsorbents at high concentrations of the metal ions [38], the limitation of the active sites of adsorbents [39], or the increase of the repel-

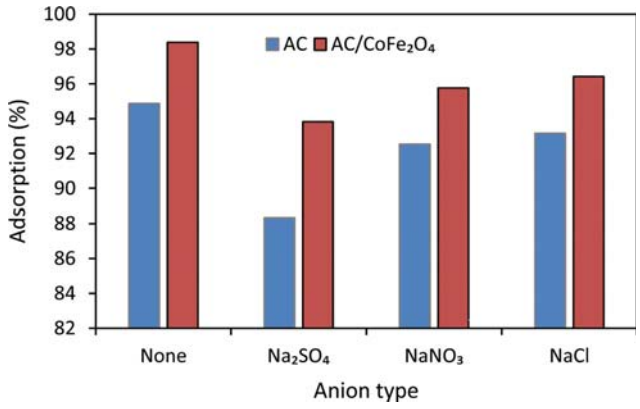

Fig. 5. The effect of various anions on the sorption efficiency of Cr(VI) using AC and AC/$CoFe_2O_4$ magnetic composite.

lant electrostatic force between the adsorbent surface and chromium (VI) in aqueous solution [40].

3-4. Effect of Co-existing Anion

Wastewaters contain various anions that may compete with anion chromium to absorb adsorption sites. Therefore, studying the effect of the co-presence of anions on the adsorption performance can be useful. Fig. 5 shows the adsorption of chromium in the presence of several anions. This figure clearly shows that when sulfate and nitrate are co-existing, the chromium sorption efficiency decreases. The overall effect of anions on adsorption efficiency is as follows: $SO_4^{2-}>NO_3^->Cl^-$. These observations suggest that anions compete with chromium ion to capture adsorption sites. These results are consistent with the findings of others [41,42], which reported that the presence of sulfate reduces the removal efficiency of chromium. In contrast, the effect of Cl^- ion on the adsorption of chromium by both adsorbents was negligible, which is consistent with the findings of others [41].

4. Desorption and Reusability

The ability to reuse adsorbents is a key factor for industrial applications of these materials. The desorption evaluation on the activated carbon and AC/$CoFe_2O_4$ magnetic adsorbent was done by using various NaOH concentrations (0.05, 0.1, 0.2, 0.3, and 0.5 M) and the contact time of 120 minutes. The results are shown in Fig. 6(a). According to the results, with increasing the concentrations of NaOH, the chromium (VI) removal by the AC and AC/$CoFe_2O_4$ magnetic composite was increased. The maximum chromium (VI) adsorption efficiency was obtained at 0.5 M NaOH concentration, and the maximum yield for AC and AC/$CoFe_2O_4$ was determined 98.44% and 98.61%, respectively.

The ability of AC prepared from *P. dactylifera* stone and AC/$CoFe_2O_4$ magnetic composite was tested in seven stages of sorption-desorption to remove chromium, and the results are plotted in Fig. 6(b). The reduction of the chromium sorption efficiency after seven times usage of adsorbents was less than 10%. Therefore, the reduction of adsorption efficiency during the adsorption-desorption process was abandoned and results indicate that activated carbon and the AC/$CoFe_2O_4$ magnetic composite has the potential to reuse for chromium removal from aqueous solutions.

5. Adsorption Isotherms

An adsorption isotherm model explains the relationship between the amount of adsorbed ions on the surface of the adsorbent and that residual adsorbate content in the water at the equilibrium [43]. Isotherm results establish the adsorption capacity of adsorbents. Langmuir, Freundlich, and Dubinin-Radushkevich (D-R) isotherm equations were tested in the present study. The fitted model was evaluated by comparing the correlation coefficient (R^2 value).

In Langmuir model, the adsorption is carried out in homogeneous and single-layer sites with the same adsorption energy [44]. In other words, adsorption can only occur in specific sites without any interaction between the molecules/ions of adsorbent and adsorbate. The linear form of Langmuir isotherm can be written as the following equation:

$$\frac{C_e}{q_e}=\frac{1}{bq_{max}}=\frac{C_e}{q_{max}} \tag{4}$$

where C_e (mg/L) is the equilibrium Cr(VI) concentration, q_{max} (mg/g) is maximum adsorption capacity, and b (L/mg) is Langmuir constant. Other important and effective parameter that characterizes the properties of the Langmuir equation is the equilibrium parameter of R_L. The value of R_L represents the state of the adsorption model. If $R_L>1$, $R_L=0$, $R_L=1$, and $0<R_L<1$, the process is undesir-

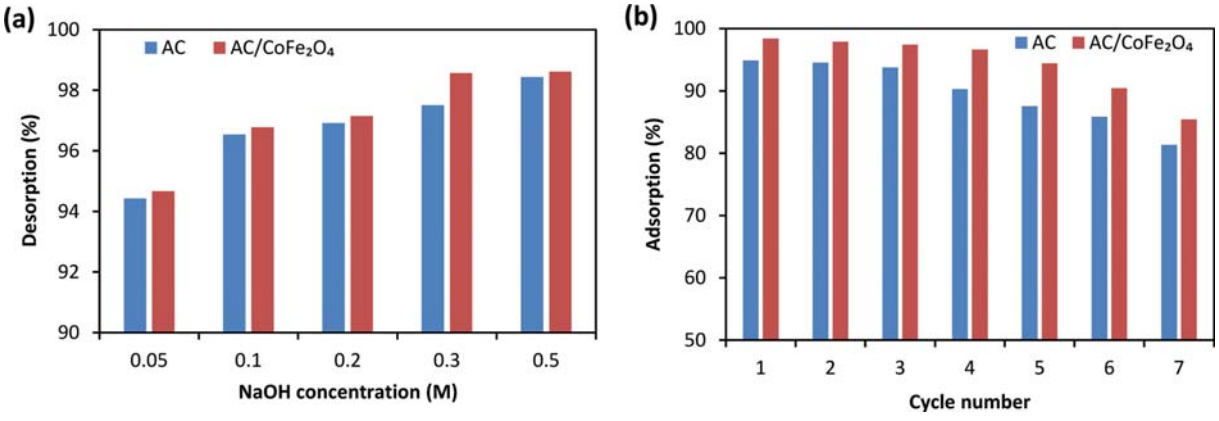

Fig. 6. (a) Effect of different concentrations of NaOH solution on chromium ion desorption and (b) Investigating the ability of adsorbents to adsorb chromium (VI) from aqueous solution.

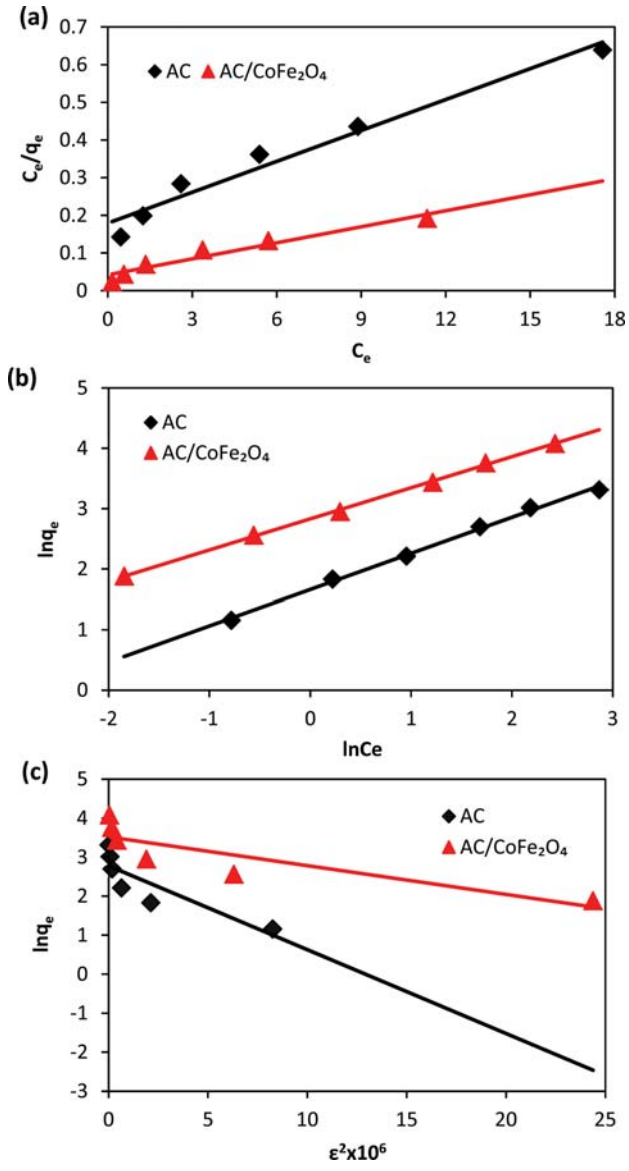

Fig. 7. Langmuir (a), Freundlich, (b) and D-R (c) isotherm models.

able, irreversible, linear, and desirable, respectively [45]. The value of R_L is determined using the following equation:

$$R_L = \frac{1}{1+bC_0} \quad (5)$$

The plot of the Langmuir model is represented in Fig. 7(a) and other details are presented in Table 1. Based on Table 1, the correlation coefficient for both the adsorbents was obtained >0.94, which shows that the Langmuir isotherm model is capable of describing adsorption data. The maximum monolayer capacity obtained from the Langmuir model for AC and AC/$CoFe_2O_4$ composite is 36.49 mg/g and 70.42 mg/g, respectively. By magnetizing the AC particles, the oxygen-containing functional groups in the AC/$CoFe_2O_4$ surface is increased and that may be contributing to the removal of heavy metals [46]. The adsorption capacity of AC and AC/$CoFe_2O_4$ composite in comparison with different adsorbents is shown in Table 2. This table indicates that AC/$CoFe_2O_4$ has a higher capacity compared with most of the sorbents. Different values of R_L were determined in the range of 0.0613-0.395 for AC and 0.028-0.228 for AC/$CoFe_2O_4$ composite. With respect to R_L values, it is concluded the Cr(VI) adsorption process is suitable and desirable.

Unlike the Langmuir model, the Freundlich model is used to describe multilayer and heterogeneous adsorption of molecules/ions onto the surface of adsorbent [47]. The empirical equation of Freundlich isotherm can be described using the following equation:

$$\ln q_e = \ln k_f + \left(\frac{1}{n}\right)\ln C_e \quad (6)$$

where k_f (mg/g (L/mg)$^{1/n}$) is the adsorption capacity factor and n is the adsorption intensity factor. The n value in the range of 1-10 indicates that the adsorption process is favorable. This parameter also expresses the physical or chemical nature of the adsorption process. If the n value is equal to unity the adsorption process is linear; if the n value is greater than 1, the process is physical and desirable; and if the n value is less than 1, the process is chemical and desirable type [48,49].

Fig. 7(b) shows Freundlich plots for the adsorption of Cr(VI). The n and k_f constants were calculated from the slope and inter-

Table 1. Results of isotherm modeling

Model	Parameters	Adsorbent	
		AC	AC/$CoFe_2O_4$
Langmuir	q_m (mg/g)	36.496	70.422
	b (L/mg)	0.153	0.337
	R^2	0.9652	0.9435
	R_L	0.0613-0.395	0.028-0.228
Freundlich	n	1.673	1.94
	k_f (mg/g (L/mg)$^{1/n}$)	5.267	16.94
	R^2	0.9968	0.9991
Dubinin-Radushkevich (D-R)	E (KJ/mol)	1.524	2.604
	q_m (mg/g)	16.057	33.733
	$\beta\times10^{-6}$ (mol^2/J^2)	0.215	0.0737
	R^2	0.7501	0.7468

Table 2. Comparison of adsorption capacity of AC and AC/$CoFe_2O_4$ composite with the various adsorbents

Adsorbent	q_{max} (mg/g)	Reference
ASGS	90.9	[50]
APT-ASEP	80.84	[51]
AC/$CoFe_2O_4$	70.42	**Present work**
Cs-g-PBA/SG	55.71	[34]
APT-SEP	52.99	[51]
Magnetic magnetite (Fe_3O_4)	52.8-53.1	[52]
Metal organic frameworks	48	[53]
Raw *Sterculia guttata* shell	45.45	[50]
Powdered activated carbon	43.29	[12]
AC	36.49	**Present work**
Magnetic $MnFe_2O_4$/chitosan nanocomposites	35.2	[54]
Modified *Sargassum oligocystum* brown algae	34.36	[33]
HCCS composite	32.99-34.92	[55]
Fe_3O_4/GO	32.33	[56]
HCAlg composite	25.23-26.80	[55]
Magnetic biochar (MMABC)	25.27	[57]
Montmorillonite (MMT)	23.9	[58]
Ulva compressa L.	21.66	[59]
Simple *Sargassum oligocystum* brown algae	21.57	[33]
Inorganic-organic clay	9.61-28.09	[60]
DAT-HDTMABr	9.12-17.03	[61]
DAT	7.04-9.09	[61]
Zirconium oxide-immobilized alginate beads	4.610-11.38	[62]
ACC	0.83	[63]

cept of the regression equation, respectively, and reported in Table 1. The n value indicates that the adsorption process is physical and desirable. The values of the correlation coefficients show that the description of adsorption equilibrium data with the Freundlich isotherm is slightly better than Langmuir isotherm.

The D-R model is more general than the Langmuir model, and it does not assume that the adsorption surface is homogeneous [50]. It has commonly been described as:

$$\ln q_e = \ln q_m - \beta\varepsilon^2 \tag{7}$$

where q_m (mg/g) is the maximum adsorption capacity, β (mol^2/J^2) is related to the adsorption energy, and ε is calculated from the $\varepsilon = RT\ln(1+1/C_e)$ equation. The results obtained from the D-R model for the chromium removal are presented in Table 1. Fig. 7(c) shows the plot of ln q_e versus ε^2 of the experimental data. The value of β parameter is used for calculating the mean free energy of adsorption (E, kJ/mol) based on the following equation:

$$E = \frac{1}{\sqrt{2\beta}} \tag{8}$$

If E=8-16 kJ/mol and E<8 kJ/mol, then the mechanism of Cr adsorption process will be the ion exchange and physical, respectively.

The correlation coefficient for the D-R model was obtained as 0.7468, which is less than Langmuir and Freundlich model. The maximum capacity is 33.73 mg/g, which is about half of the q_m obtained by Langmuir isotherm (70.42 mg/g). Considering the amount of mean adsorption energy, it was concluded that the chromium (VI) adsorption process using AC and AC/$CoFe_2O_4$ composite is physical.

6. Kinetic Study

Determination of kinetic parameters to predict the rate of adsorption reactions is useful and provides valuable information about the mechanism of adsorption [64]. In this work, two kinetic models, pseudo-first-order (Eq. (8)) and pseudo-second-order (Eq. (9)), were applied to obtain the best kinetic model that will describe the experimental data.

$$\ln(q_e - q_t) = \ln q_e - t\,k_1 \tag{9}$$

$$\frac{t}{q_t} = \left(\frac{1}{k_2 q_e^2}\right) + \frac{t}{q_e} \tag{10}$$

where q_t (mg/g) is the amount of chromium adsorbed to the specific amount of adsorbent at a given time t, k_1 (min^{-1}) is the equilibrium rate constant of the pseudo-first-order model, and k_2 (g/mg min) is the rate constant of pseudo-second-order model.

Results of kinetic modeling are presented in Fig. 8 and Table 3. As seen in Table 3, the correlation coefficient, R^2, for the pseudo-second-order kinetic model is higher than pseudo-first-order, indicating that the experimental adsorption data was well fitted with the pseudo-second-order model. Further, the closeness of $q_{e.Cal}$ to $q_{e.exp}$ values in the pseudo-second-order model is reconfirmation of the suitability of this model to describe data. By increasing the initial concentration of chromium, the rate constant of k_2 is reduced, which can be attributed to the increasing the concentration of

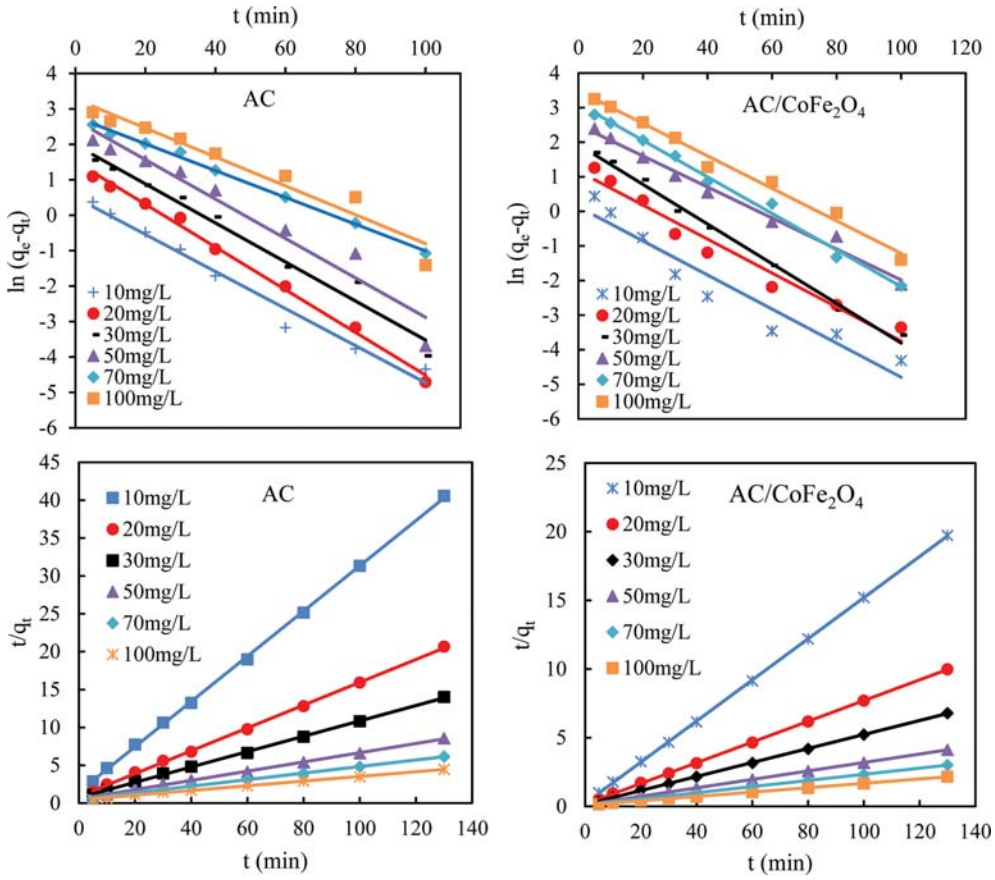

Fig. 8. Pseudo-first order and pseudo-second order models for Cr(VI) adsorption by AC and AC/$CoFe_2O_4$ composite.

Table 3. Kinetic modeling results

Adsorbent	Kinetic model	Parameters	Cr(VI) concentration (mg/L)					
			10	20	30	50	70	100
AC	Pseudo-first-order	$q_{e.\,Cal}$	1.65	4.52	7.27	14.54	15.99	32.48
		k_1	0.052	0.060	0.055	0.055	0.037	0.047
		R^2	0.9784	0.9952	0.9767	0.9461	0.9967	0.9873
	Pseudo-second-order	$q_{e.\,Cal}$	3.34	6.63	9.86	16.62	23.14	62.89
		k_2	0.060	0.025	0.014	0.006	0.003	0.002
		R^2	0.9996	0.9994	0.9993	0.9986	0.9979	0.9996
		$q_{e.\,exp}$	3.20	6.29	9.28	15.21	21.17	60.06
AC/$CoFe_2O_4$	Pseudo-first-order	$q_{e.\,Cal}$	1.13	3.18	6.86	12.16	22.26	32.48
		k_1	0.049	0.049	0.057	0.044	0.052	0.047
		R^2	0.9192	0.9624	0.9937	0.9866	0.9934	0.9873
	Pseudo-second-order	$q_{e.\,Cal}$	6.68	13.26	19.64	32.46	44.84	62.89
		k_2	0.099	0.035	0.019	0.008	0.005	0.002
		R^2	0.9999	0.9999	0.9999	0.9999	0.9997	0.9996
		$q_{e.\,exp}$	6.59	13.02	19.16	31.57	43.13	60.06

hexavalent chromium compared to the effectively available sites of the adsorbents in the solution.

The adsorption performance of Cr(VI) onto AC and AC/$CoFe_2O_4$ was also calculated based on the $q_{e.\,cal}$ and k_2 parameters of the pseudo-second-order model at the solution temperature of 25 °C (Eqs. (11)-(14)) [49]:

$$R_w = \frac{1}{1 + K_2 q_e t_w} \quad (11)$$

$$R_i = k_2 q_e \quad (12)$$

Table 4. Required operating times for various fractional adsorption values

Adsorbent	Operating time, t_x	Fractional adsorption, X	Value (min)
AC	$t_{0.544}$	0.54	6.17
	$t_{0.674}$	0.67	10.70
	$t_{0.806}$	0.80	21.52
	$t_{0.881}$	0.88	38.35
	$t_{0.943}$	0.94	85.71
	$t_{0.986}$	0.98	364.91
	$t_{0.992}$	0.99	642.48
	$t_{0.996}$	0.99	1290.15
$AC/CoFe_2O_4$	$t_{0.764}$	0.76	4.92
	$t_{0.853}$	0.85	8.83
	$t_{0.928}$	0.92	19.61
	$t_{0.975}$	0.97	59.36
	$t_{0.986}$	0.98	107.19
	$t_{0.9951}$	0.99	259.40
	$t_{0.9955}$	0.99	336.71
	$t_{0.997}$	0.99	505.83

$$t_{1/2}=\frac{1}{k_2 q_e} \quad (13)$$

$$t_x=\frac{S}{k_2 q_e} \quad (14)$$

where R_i (min^{-1}) is the index of second-order rate, R_w the factor of approaching equilibrium, t_w (min) is the longest reaction time, $t_{1/2}$ (min) is the required reaction time for arriving the initial Cr(VI) content to the half level by AC and $AC/CoFe_2O_4$ composite, t_x (min) is the required contact time for the determined value of fractional sorption ($X=q_t/q_e$), and S is equivalent to 'X/(1−X)'. If the amount of R_w fits the ranges of <0.01, 0.1-0.01, and 0.1-1, then the kinetic is evaluated as drastically approaching equilibrium, well-approaching equilibrium, and slightly approaching equilibrium, respectively.

As seen in Table 4, the value of R_w was 0.0383 and 0.0115 for AC and $AC/CoFe_2O_4$ composite, respectively. It was revealed that the chromium adsorption process well arrived at the equilibrium level. The level of R_i and $t_{1/2}$ factors was also 0.193 min^{-1} and 5.18 min for AC and 0.657 min^{-1} and 1.52 min for $AC/CoFe_2O_4$ composite, respectively. The small value of half-life for $AC/CoFe_2O_4$ composite reveals its high adsorption rate. R_i is a key parameter influencing the amount of fractional adsorption. Thus, it was used to calculate the data of t_x for various X values of Cr(VI) adsorption by AC and $AC/CoFe_2O_4$ composite, and the results are depicted in Table 4. Generally, these findings would be useful for designing the Cr(VI) adsorption process by AC and $AC/CoFe_2O_4$.

7. Effect of Temperature and Thermodynamic Study

The removal of Cr(VI) at different temperatures in the range of 25-55 °C was evaluated, and results are shown in Fig. 9(a). It was observed that by increasing the temperature the removal efficiency slightly decreased. Lower temperature was found to be favorable for chromium removal. This result affirms the exothermic character of the adsorption process.

The thermodynamic parameters including Gibbs free energy change (ΔG^o, kJ/mol), enthalpy (ΔH^o, kJ/mol), and entropy (ΔS^o, J/mol K) were calculated for the process using Eqs. (15)-(17):

$$\Delta G^o=-RT\ln k_D \quad (15)$$

$$k_D=\frac{q_e}{C_e} \quad (16)$$

$$\ln k=\frac{-\Delta G^o}{RT}=\frac{-\Delta H^o}{RT}+\frac{\Delta S^o}{R} \quad (17)$$

Where R, k_D, and T are the universal gas constant (8.314 J/mol K), equilibrium constant, and solution temperature, respectively. Plot of ln k_D versus 1/T gives the values of ΔH^o and ΔS^o (Fig. 9(b)). The obtained parameters are shown in Table 5. The negative values of ΔG^o in the range of −4.50 to 3.76 for AC and −9.17 to −7.66 for $AC/CoFe_2O_4$ magnetic composite suggest the spontaneous nature of the Cr adsorption process. The negative value of ΔH^o implies the exothermic character of adsorption, and the negative value of ΔS^o illustrated enthalpy driven of the reaction and reduced randomness at the interface of the solid/solution.

CONCLUSION

Phoenix dactylifera activated carbon (AC) was successfully com-

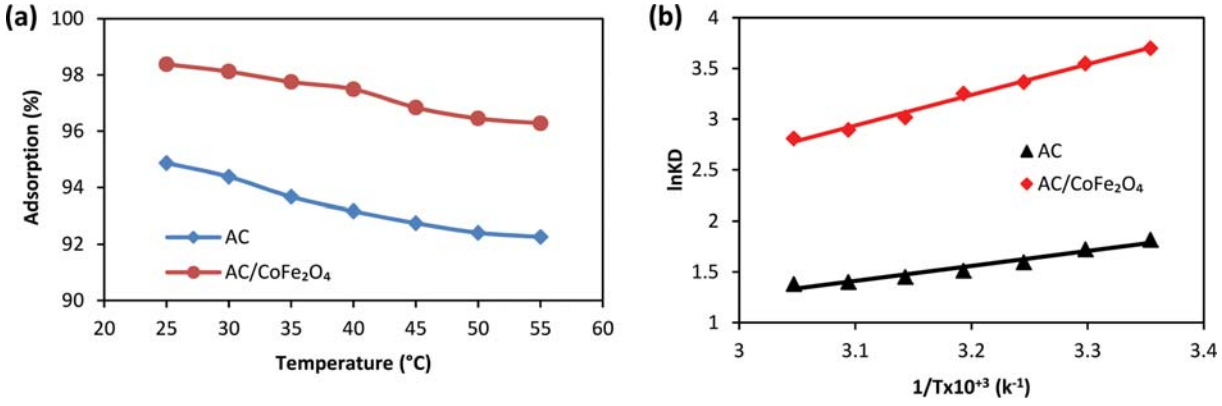

Fig. 9. Effect of temperature on Cr(VI) adsorption (a) and plot of lnk_D *vs* 1/T for determining thermodynamic parameters (b).

Table 5. Thermodynamic parameters

Adsorbent	T (°C)	ΔG^o (kJ/mol)	ΔH^o (kJ/mol)	ΔS^o (J/mol·K)
AC	25	−4.50	−12.29	−26.39
	30	−4.34		
	35	−4.08		
	40	−3.93		
	45	−3.83		
	50	−3.76		
	55	−3.76		
$AC/CoFe_2O_4$	25	−9.17	−25.13	−53.51
	30	−8.94		
	35	−8.62		
	40	−8.46		
	45	−7.98		
	50	−7.78		
	55	−7.66		

posited with $CoFe_2O_4$ to make a novel adsorbent of $AC/CoFe_2O_4$ magnetic composite. The Cr(VI) removal performance of both $AC/CoFe_2O_4$ magnetic composite and AC was evaluated. FTIR analysis showed that all the functional groups in the $AC/CoFe_2O_4$ magnetic composite played a significant role in the adsorption of Cr(VI) ions. From XRD patterns it was revealed that the $AC/CoFe_2O_4$ magnetic composite has a crystalline structure. Addition of $CoFe_2O_4$ nanoparticles has a significant effect on the thermal stability of activated carbon. The experimental results showed that pH, initial Cr(VI) concentration, contact time, and dosage had a marked impact on the chromium removal. After seven times of adsorption-desorption, both adsorbents were efficiently adsorbing chromium ions. The most effective tested co-presented anions that interfere with the adsorption of Cr(VI) were sulfate. The small value of half-life ($t_{1/2}$=1.52 min) for $AC/CoFe_2O_4$ composite revealed its high adsorption rate. Chromium adsorption data were more consistent with the Freundlich isotherm and pseudo-second-order kinetic. The reaction of chromium with adsorbents was spontaneous and exothermic.

ACKNOWLEDGEMENT

This work has been extracted from the thesis of R. Foroutan. Hereby, the authors acknowledge the technical and financial support provided by the University of Tabriz (Grant No. Tab-1132-96) to conduct this work.

REFERENCES

1. X. Jiang, Q.-D. An, Z.-Y. Xiao, S.-R. Zhai and Z. Shi, *Mater. Res. Bull.*, **102**, 218 (2018).
2. M. Ahmadi, E. Kouhgardi and B. Ramavandi, *Korean J. Chem. Eng.*, **33**, 2589 (2016).
3. H. Liu, Z. Wang, H. Li, H. Wang and R. Yu, *Mater. Res. Bull.*, **100**, 302 (2018).
4. J. Yu, C. Jiang, Q. Guan, P. Ning, J. Gu, Q. Chen, J. Zhang and R. Miao, *Chemosphere*, **195**, 632 (2018).
5. C. Sakulthaew, C. Chokejaroenrat, A. Poapolathep, T. Satapanajaru and S. Poapolathep, *Chemosphere*, **184**, 1168 (2017).
6. R. Jobby, P. Jha, A. K. Yadav and N. Desai, *Chemosphere*, **207**, 255 (2018).
7. J. Zhou, Y. Wang, J. Wang, W. Qiao, D. Long and L. Ling, *J. Colloid Interface Sci.*, **462**, 200 (2016).
8. N. Ranjbar, S. Hashemi, B. Ramavandi and M. Ravanipour, *Environ. Prog. Sustain. Energy* (2018), https://doi.org/10.1002/ep.12854.
9. E. I. Basaldella, P. G. Vázquez, F. Iucolano and D. Caputo, *J. Colloid Interface Sci.*, **313**, 574 (2007).
10. Y. Zhao, S. Yang, D. Ding, J. Chen, Y. Yang, Z. Lei, C. Feng and Z. Zhang, *J. Colloid Interface Sci.*, **395**, 198 (2013).
11. W. Yu, L. Zhang, H. Wang and L. Chai, *J. Hazard. Mater.*, **260**, 789 (2013).
12. W. Wang, *Chemosphere*, **190**, 97 (2018).
13. I. Enniya, L. Rghioui and A. Jourani, *Sustain Chem. Pharm.*, **7**, 9 (2018).
14. S. Norouzi, M. Heidari, V. Alipour, O. Rahmanian, M. Fazlzadeh, F. Mohammadi-moghadam, H. Nourmoradi, B. Goudarzi and K. Dindarloo, *Bioresour. Technol.*, **258**, 48 (2018).
15. L. Niazi, A. Lashanizadegan and H. Sharififard, *J. Clean Prod.*, **185**, 554 (2018).
16. M. S. Gaikwad and C. Balomajumder, *Chemosphere*, **184**, 1141 (2017).
17. K. K. Senapati, C. Borgohain and P. Phukan, *J. Mol. Catal. A*, **339**, 24 (2011).
18. V. Srivastava, T. Kohout and M. Sillanpää, *J. Environ. Chem. Eng.*, **4**, 2922 (2016).
19. C. Wan and J. Li, *Carbohyd. Polym.*, **134**, 144 (2015).
20. T. G. Glover, D. Sabo, L. A. Vaughan, J. A. Rossin and Z. J. Zhang, *Langmuir*, **28**, 5695 (2012).
21. W. Qiu, D. Yang, J. Xu, B. Hong, H. Jin, D. Jin, X. Peng, J. Li, H. Ge and X. Wang, *J. Alloys Compd.*, **678**, 179 (2016).
22. T. M. Darweesh and M. J. Ahmed, *Environ. Toxicol. Phar.*, **50**, 159 (2017).
23. D. Pathania, A. Sharma and Z.-M. Siddiqi, *J. Mol. Liq.*, **219**, 359 (2016).
24. Y. Gao, Q. Yue, B. Gao, Y. Sun, W. Wang, Q. Li and Y. Wang, *Chem. Eng. J.*, **232**, 582 (2013).
25. S. Ayyappan, S. Mahadevan, P. Chandramohan, M. Srinivasan, J. Philip and B. Raj, *J. Phys. Chem. C*, **114**, 6334 (2010).
26. M. Rai, G. Shahi, V. Meena, R. Meena, S. Chakraborty, R. Singh and B. Rai, *Resource-Efficient Technol.*, **2**, S63 (2016).
27. Q.-Q. Zhong, Q.-Y. Yue, Q. Li, B.-Y. Gao and X. Xu, *Carbohyd. Polym.*, **111**, 788 (2014).
28. W. M. Ibrahim, A. F. Hassan and Y. A. Azab, *Egypt. J. Basic Appl. Sci.*, **3**, 241 (2016).
29. A. F. Hassan and A. M. Youssef, *Carbon Let.*, **15**, 57 (2014).
30. M. López-López, J. Durán, A. Delgado and F. González-Caballero, *J. Colloid Interface Sci.*, **291**, 144 (2005).
31. R. Fu, Y. Liu, Z. Lou, Z. Wang, S. A. Baig and X. Xu, *J. Taiwan Inst. Chem. Eng.*, **62**, 247 (2016).
32. S. Li, L. Liu, Y. Yu, G. Wang, H. Zhang and A. Chen, *J. Alloys Compd.*, **698**, 20 (2017).
33. R. Foroutan, R. Mohammadi and B. Ramavandi, *Korean J. Chem. Eng.*, **35**, 234 (2018).

34. R. Nithya, T. Gomathi, P. Sudha, J. Venkatesan, S. Anil and S.-K. Kim, *Int. J. Biol. Macromol.*, **87**, 545 (2016).
35. R. Foroutan, F. S. Khoo, B. Ramavandi and S. Abbasi, *Desalin. Water Treat.*, **82**, 146 (2017).
36. B. Naeimi, R. Foroutan, B. Ahmadi, F. Sadeghzadeh and B. Ramavandi, *Mater. Res. Exp.*, **5**, 045501 (2018).
37. M. Vieira, A. A. Neto, M. Gimenes and M. Da Silva, *J. Hazard. Mater.*, **177**, 362 (2010).
38. V. Singh, A. Sharma, D. Tripathi and R. Sanghi, *J. Hazard. Mater.*, **161**, 955 (2009).
39. O. Acisli, A. Khataee, S. Karaca and M. Sheydaei, *Ultrason. Sonochem.*, **31**, 116 (2016).
40. M. Ghaedi, A. G. Nasab, S. Khodadoust, M. Rajabi and S. Azizian, *J. Ind. Eng. Chem.*, **20**, 2317 (2014).
41. M. Gheju, I. Balcu and G. Mosoarca, *J. Hazard. Mater.*, **310**, 270 (2016).
42. S. Barnie, J. Zhang, H. Wang, H. Yin and H. Chen, *Chemosphere*, **212**, 209 (2018).
43. Z. Ding, W. Wang, Y. Zhang, F. Li and J. P. Liu, *J. Alloys Compd.*, **640**, 362 (2015).
44. I. Langmuir, *J. Am. Chem. Soc.*, **40**, 1361 (1918).
45. R. Foroutan, H. Esmaeili, S. D. Rishehri, F. Sadeghzadeh, S. Mirahmadi, M. Kosarifard and B. Ramavandi, *Data in Brief*, **12**, 485 (2017).
46. M. H. Fatehi, J. Shayegan, M. Zabihi and I. Goodarznia, *J. Environ. Chem. Eng.*, **5**, 1454 (2017).
47. H. Freundlich, *Z. Phys. Chem.*, **57**, 385 (1907).
48. B. Ramavandi, A. Rahbar and S. Sahebi, *Desal. Water Treat.*, **57**, 23814 (2016).
49. A. Teimouri, H. Esmaeili, R. Foroutan and B. Ramavandi, *Korean J. Chem. Eng.*, **35**, 479 (2018).
50. S. Rangabhashiyam and N. Selvaraju, *J. Mol. Liq.*, **207**, 39 (2015).
51. V. Marjanović, S. Lazarević, I. Janković-Častvan, B. Jokić, D. Janaćković and R. Petrović, *Appl. Clay Sci.*, **80**, 202 (2013).
52. S. Rajput, C. U. Pittman Jr. and D. Mohan, *J. Colloid Interface Sci.*, **468**, 334 (2016).
53. A. Maleki, B. Hayati, M. Naghizadeh and S. W. Joo, *Ind. Eng. Chem. Res.*, **28**, 211 (2015).
54. Y. Xiao, H. Liang and Z. Wang, *Mater. Res. Bull.*, **48**, 3910 (2013).
55. S. Periyasamy and N. Viswanathan, *New J. Chem.*, **42**, 3371 (2018).
56. M. Liu, T. Wen, X. Wu, C. Chen, J. Hu, J. Li and X. Wang, *Dalton Trans.*, **42**, 14710 (2013).
57. X. Zhang, L. Lv, Y. Qin, M. Xu, X. Jia and Z. Chen, *Bioresour. Technol.*, **256**, 1 (2018).
58. H. Uslu, D. Datta and S. Azizian, *J. Mol. Liq.*, **215**, 449 (2016).
59. A. Aid, S. Amokrane, D. Nibou, E. Mekatel, M. Trari and V. Hulea, *Water Sci. Technol.*, **77**, 60 (2018).
60. S. I. Rathnayake, W. N. Martens, Y. Xi, R. L. Frost and G. A. Ayoko, *J. Colloid Interface Sci.*, **490**, 163 (2017).
61. R. A. Abu-Zurayk, R. Z. Al Bakain, I. Hamadneh and A. H. Al-Dujaili, *Int. J. Miner. Proces*, **140**, 79 (2015).
62. R. Kumar, S.-J. Kim, K.-H. Kim, S.-h. Lee, H.-S. Park and B.-H. Jeon, *Appl. Geochem.*, **88**, 113 (2018).
63. P. Maneechakr and S. Karnjanakom, *J. Chem. Thermodyn.*, **106**, 104 (2017).
64. J. Yang, M. Yu and W. Chen, *Ind. Eng. Chem. Res.*, **21**, 414 (2015).